FIGL1 prevents aberrant chromosome associations and fragmentation and limits crossovers in polyploid wheat meiosis

Osman, Kim; Desjardins, Stuart D.; Simmonds, James; Burridge, Amanda J.; Kanyuka, Kostya; Henderson, Ian R.; Edwards, Keith J.; Uauy, Cristobal; Franklin, F. Chris H.; Higgins, James D.; Sanchez-Moran, Eugenio

DOI:
10.1111/nph.19716

New Phytologist

Research

FIGL1 prevents aberrant chromosome associations and fragmentation and limits crossovers in polyploid wheat meiosis

Kim Osman[1]*, Stuart D. Desjardins[2]*, James Simmonds[3], Amanda J. Burridge[4], Kostya Kanyuka[5], Ian R. Henderson[6], Keith J. Edwards[4], Cristobal Uauy[3], F. Chris H. Franklin[1], James D. Higgins[2] and Eugenio Sanchez-Moran[1]

[1]School of Biosciences, University of Birmingham, Edgbaston, Birmingham, B15 2TT, UK; [2]Department of Genetics and Genome Biology, University of Leicester, University Road, Adrian Building, Leicester, LE1 7RH, UK; [3]John Innes Centre, Norwich Research Park, Norwich, NR4 7UH, UK; [4]Life Sciences Building, University of Bristol, 24 Tyndall Avenue, Bristol, BS8 1TQ, UK; [5]NIAB, 93 Lawrence Weaver Rd, Cambridge, CB3 0LE, UK; [6]Department of Plant Sciences, University of Cambridge, Downing Street, Cambridge, CB2 3EA, UK

Authors for correspondence:
Kim Osman
Email: k.osman@bham.ac.uk

Eugenio Sanchez-Moran
Email: e.sanchez-moran@bham.ac.uk

James D. Higgins
Email: jh555@leicester.ac.uk

Received: *16 October 2023*
Accepted: *10 March 2024*

New Phytologist (2024)
doi: 10.1111/nph.19716

Key words: chromosomes, FIGL1, genetic crossovers, meiosis, polyploid, recombination, *Triticum*, wheat.

Summary

- Meiotic crossovers (COs) generate genetic diversity and are crucial for viable gamete production. Plant COs are typically limited to 1–3 per chromosome pair, constraining the development of improved varieties, which in wheat is exacerbated by an extreme distal localisation bias. Advances in wheat genomics and related technologies provide new opportunities to investigate, and possibly modify, recombination in this important crop species. Here, we investigate the disruption of *FIGL1* in tetraploid and hexaploid wheat as a potential strategy for modifying CO frequency/position.
- We analysed *figl1* mutants and virus-induced gene silencing lines cytogenetically. Genetic mapping was performed in the hexaploid.
- FIGL1 prevents abnormal meiotic chromosome associations/fragmentation in both ploidies. It suppresses class II COs in the tetraploid such that CO/chiasma frequency increased 2.1-fold in a *figl1 msh5* quadruple mutant compared with a *msh5* double mutant. It does not appear to affect class I COs based on HEI10 foci counts in a hexaploid *figl1* triple mutant. Genetic mapping in the triple mutant suggested no significant overall increase in total recombination across examined intervals but revealed large increases in specific individual intervals.
- Notably, the tetraploid *figl1* double mutant was sterile but the hexaploid triple mutant was moderately fertile, indicating potential utility for wheat breeding.

Introduction

Meiosis is a specialised form of cell division in which DNA replication is followed by two sequential rounds of cell division to halve the chromosome number during gamete formation. During meiotic prophase I, the programmed formation of numerous DNA double-strand breaks (DSBs) catalysed by the SPO11 complex (Keeney *et al.*, 1997; Vrielynck *et al.*, 2016), followed by repair of the breaks by homologous recombination (HR), results in either noncrossovers (NCOs) or crossovers (COs; Börner *et al.*, 2004). COs involve reciprocal genetic exchanges between the maternal and paternal chromosomes, which generate genetic variation and form physical links between homologous chromosomes that are essential for accurate segregation at the first meiotic division. In plants, COs can form via either of two pathways (Osman *et al.*, 2011; Mercier *et al.*, 2015; Wang & Copenhaver, 2018; Desjardins *et al.*, 2020). The class I pathway accounts for *c.* 85% of all COs in plants and involves the activities of a group of recombination proteins known as ZMMs: Zip2/SHOC1, Zip3/HEI10, ZIP4, MER3/RCK, MSH4, MSH5 and PTD (Higgins *et al.*, 2004, 2005, 2008b; Mercier *et al.*, 2005; Wijeratne *et al.*, 2006; Chelysheva *et al.*, 2007, 2012; Macaisne *et al.*, 2008, 2011). Class I COs are interference-sensitive leading them to be well-spaced along chromosomes (Jones & Franklin, 2006; Martini *et al.*, 2006). The remaining COs (Class II) are insensitive to interference and are partly dependent on the activity of the MUS81 endonuclease (Berchowitz *et al.*, 2007; Higgins *et al.*, 2008a,b).

HR is accompanied by remodelling of the meiotic chromosomes and the two processes are tightly integrated (Zickler & Kleckner, 2023). Following the premeiotic S-phase, sister chromatids are held together by cohesin proteins (Haering & Jessberger, 2012) and during leptotene become organised into linear looped arrays whose bases are anchored by the elaboration of a proteinaceous chromosome axis (Zickler & Kleckner, 2023). During zygotene, aligned homologous chromosomes are brought into close apposition by the formation of the synaptonemal

*These authors contributed equally to this work.

complex (SC), which has a tri-partite structure, comprising the chromosome axes (now referred to as lateral elements) and cross-linking, transverse filament proteins (Page & Hawley, 2004). At pachytene, the SC is fully polymerised along the chromosomes and during diplotene, when CO formation is complete, the SC disassembles and chromosomes begin to condense. Condensation continues through diakinesis when homologue pairs become apparent as bivalent structures linked by one or more chiasmata, which are the cytological manifestation of COs. By metaphase I, chromosomes are fully condensed and attach to the meiotic spindle in preparation for segregation of the homologues at the first meiotic division. A second nonreductional division separates the sister chromatids producing the four haploid products of meiosis.

Meiotic recombination is tightly controlled at multiple levels, and in plants, the vast majority of initiating DSBs are not repaired as COs, typically resulting in only one to three COs per homologue pair, regardless of chromosome size (Mercier *et al.*, 2015). For example, hexaploid wheat produces *c.* 2000 DSBs but only *c.* 42 COs per male meiosis (Gardiner *et al.*, 2019; Osman *et al.*, 2021; Higgins *et al.*, 2022). The constraints on CO frequency impose severe limitations on plant breeding programmes and are exacerbated by localisation bias in some large genome crop species, particularly cereals where the majority of recombination events take place in proximity to the chromosome ends, making it very difficult to introgress useful agronomic traits into more interstitial and centromere proximal regions (Saintenac *et al.*, 2009; Choulet *et al.*, 2014). For example, cytological estimates indicate a 25 : 1 bias towards distal chiasmata in barley and a 9 : 1 bias in hexaploid wheat (Higgins *et al.*, 2012; Osman *et al.*, 2021). The discovery of several recombination-limiting mechanisms in Arabidopsis has therefore generated much interest, suggesting possible routes for modifying CO frequency and/or location in crop species. For example, class I COs are limited by HEI10 dosage (Ziolkowski *et al.*, 2017); *HCR1*, which encodes the protein phosphatase PPX1, (Nageswaran *et al.*, 2021); and the presence of the SC transverse filament protein, ZYP1a/ZYP1b, (Capilla-Pérez *et al.*, 2021; France *et al.*, 2021). Class II COs are limited by several independent anti-recombination pathways including the FANCM helicase (Crismani *et al.*, 2012; Knoll *et al.*, 2012); RECQ4 helicase (Séguéla-Arnaud *et al.*, 2015); and FIGL1, a conserved AAA-ATPase, (Girard *et al.*, 2015). Furthermore, it appears that simultaneous disruption of multiple recombination-limiting mechanisms in Arabidopsis can produce synergistic effects leading to substantial increases in recombination frequency (Girard *et al.*, 2015; Serra *et al.*, 2018; Fernandes *et al.*, 2018a; Durand *et al.*, 2022).

To date, attempts to reproduce these pro-CO strategies in crop species have had varying success. Mutation of *RECQ4* has increased CO frequency in all species tested, including rice, pea, tomato (all in hybrid contexts) and barley, suggesting that this may be a universal tool for increasing recombination frequency in plants (Mieulet *et al.*, 2018; Arrieta *et al.*, 2021). *FANCM* disruption increased recombination in hybrid rice, hybrid pea and in a pure line of *Brassica rapa* (Mieulet *et al.*, 2018; Blary & Jenczewski, 2019), while in wheat, FANCM was revealed to play a dual role in promoting class I COs and suppressing class II COs, resulting in an overall 31% increase in CO frequency in *fancm* hexaploid mutants, suggesting it could be an effective tool for accelerating breeding programmes (Desjardins *et al.*, 2022). In contrast, disruption of *FIGL1* (*FIGNL1* in rice) resulted in sterility in rice, pea and tomato (Zhang *et al.*, 2017; Mieulet *et al.*, 2018) but maize *figl1* mutants remained fertile, similar to the situation in Arabidopsis (T. Zhang *et al.*, 2023). Rice FIGNL1 limits class II COs and inhibits non-homologous chromosome associations, such that *fignl1* mutants display abnormal chromosome bridges and fragmentation at the division stages of meiosis, leading to the formation of inviable gametes and accounting for the infertility of these lines (Yang *et al.*, 2022). *Os*FIGNL1 and *At*FIGL1 together with their interacting partners, MEICA1 and FLIP respectively, act at the strand invasion stage of meiosis (Hu *et al.*, 2017; Fernandes *et al.*, 2018b; Yang *et al.*, 2022). Maize FIGL1 also appears to act at this stage but whereas *At*FIGL1 negatively regulates recombination, acting antagonistically with BRCA2 to modulate RAD51/DMC1 dynamics (Girard *et al.*, 2015; Kumar *et al.*, 2019), *Zm*FIGL1 and *Zm*BRCA2 act co-ordinately to promote CO formation (T. Zhang *et al.*, 2023).

To the best of our knowledge, *FIGL1* has not previously been studied in a polyploid crop species. Here, we investigate the effects of disrupting *FIGL1* function in wheat using tetraploid (*Triticum turgidum*) and hexaploid (*Triticum aestivum*) mutant lines and virus-induced gene silencing (VIGS). We show that wheat FIGL1 limits COs and prevents aberrant chromosome associations and fragmentation. However, whereas mutation of FIGL1 in the tetraploid results in almost complete sterility, wheat hexaploid *figl1* plants retain a moderate degree of fertility, suggesting its higher ploidy level may confer resilience to chromosomal damage. Furthermore, genetic mapping in the triple mutant reveals perturbation of the landscape of recombination, which may be useful for plant breeding.

Materials and Methods

Wheat *FIGL1* orthologues

Wheat FIGL1 orthologues were identified using the amino acid (AA) sequences from *Arabidopsis thaliana* (GenBank: KM055500, Girard *et al.*, 2015) and *Oryza sativa* Os12g0443800 as queries to BLAST the *Triticum turgidum* L. tetraploid (Maccaferri *et al.*, 2019; Svevo.v1 http://plants.ensembl.org/Triticum_turgidum) and the *Triticum aestivum* L. hexaploid (International Wheat Genome Sequencing Consortium (IWGSC), 2018; http://plants.ensembl.org/Triticum_aestivum) genomes. All hexaploid sequences were full-length. Both tetraploid sequences were represented by several overlapping transcripts, which covered the entire coding sequence based on comparison with the *T. aestivum*, Arabidopsis and rice orthologues and so were assumed to be full-length. The *T. turgidum* reference sequence is still in its first version so the representation of FIGL1 as overlapping transcripts is most likely due to mis-annotation or incomplete assembly. Amino acid sequences

were aligned using Clustal Omega for multiple sequences (https://www.ebi.ac.uk/Tools/msa/clustalo/) or EMBOSS Needle for pairwise alignments (https://www.ebi.ac.uk/Tools/psa/) using default settings. Conserved domains were identified by searching against the CD database at https://www.ncbi.nlm.nih.gov/ apart from the predicted FRBD (FIGNL1 RAD51 Binding Domain), first described in human FIGNL1 (Yuan & Chen, 2013), which was identified by alignment with the Arabidopsis and rice sequence. The tetraploid wheat *FIGL1* genes correspond to *TtFIGL1-A1* (*TRITD5Av1G073320*) and *TtFIGL1-B1* (*TRITD5Bv1G056690*), whereas the hexaploid wheat *FIGL1* genes correspond to *TaFIGL1-A1* (TraesCS5A02G109500), *TaFIGL1-B1* (TraesCS5B02G110300) and *TaFIGL1-D1* (TraesCS5D02G123800).

Plant material

We selected mutants from the original annotation of the EMS-induced mutant lines to the Chinese Spring Survey Sequence (CSS; International Wheat Genome Sequencing Consortium, IWGSC, 2014), which was the only genome assembly available at the time (December 2015). As described above, we used the Arabidopsis and rice *FIGL1/FIGNL1* sequence to identify the wheat orthologues in the CSS annotation (Traes_5AS_68FB50ED1, Traes_5BS_01D245E9C and Traes_5DS_64BDFB2CF) and select mutants for each homoeologue in tetraploid *T. turgidum* cv 'Kronos' and hexaploid *T. aestivum* cv 'Cadenza' mutant populations (Krasileva *et al.*, 2017; Supporting Information Table S1). For tetraploid wheat, we selected premature termination codon mutants in *TtFIGL1-A1*: Kronos2408 (hereafter referred to as K2408) mutated at AA residue 253 and K2273 (at residue 410). Similarly, a premature termination codon mutant and a splice acceptor site variant were selected in *TtFIGL1-B1*: K2398 (residue 326) and K2644 (exon 7), respectively. The single mutants were crossed together to generate two independent double mutants: *Ttfigl1-1* (K2273 × K2644) and *Ttfigl1-2* (K2408 × K2398). *Ttfigl1-1* was further crossed with *Ttmsh5* (K863; Desjardins *et al.*, 2022) to generate a quadruple mutant (*Ttfigl1-1 Ttmsh5*). For hexaploid wheat, we selected the following premature termination codon mutants: *TaFIGL1-A1*: Cadenza0654 (hereafter referred to as C0654) mutated at residue 429; *TaFIGL1-B1*: C0900 (residue 326) and *TaFIGL1-D1*: C2036 (residue 326). The single mutants were crossed to generate a *Tafigl1* triple mutant (C0654 × C0900 × C2036). We confirmed all mutations by genotyping with homoeologue-specific KASP assays using published protocols (Adamski *et al.*, 2021; Table S2). Upon the subsequent publication of the IWGSC RefSeqv1.1 annotations (IWGSC, 2018), the EMS mutants were reannotated using the TraesCS5A02G109500, TraesCS5B02G110300 and TraesCS5D02G123800 gene models. The A and D genome mutants selected were re-identified in their expected position, but the B genome mutants were not called by the automated pipeline. However, the premature termination codon and splicing acceptor variants were confirmed by Sanger sequencing in lines K2398 and K2644, respectively, confirming that they are bona-fide mutants in *TtFIGL1-B1*. In all experiments, the original cultivars Kronos and Cadenza were used as wild-type (WT) controls for the tetraploid and hexaploid EMS-induced TILLING mutants, respectively (Krasileva *et al.*, 2017). All lines were obtained from the Germplasm Resources Unit (https://www.seedstor.ac.uk/shopping-cart-tilling.php). Plants were grown in a controlled environment with photoperiod 16 h; temperature 20°C and relative humidity 60%. VIGS experiments were performed in a Level 3 biological containment facility at Rothamsted Research.

Cytological procedures

Meiotic chromosome spreads were prepared from anthers fixed at the required stage of meiosis in cold ethanol : acetic acid in the ratio 3 : 1 by volume. For slide preparation, anthers were digested in 0.3% cellulase, 0.3% pectolyase, 10 mM citrate buffer, pH 4.5 at 37°C for 90 min then three anthers per slide were macerated in 70% acetic acid and incubated for 1 min on a 45°C hotplate before fixing with 130 µl cold 3 : 1 fix. Slides were either viewed directly by applying 5 µg ml^{-1} 4′,6′-diamidino-2-phenylindole (DAPI) in Vectashield (Vector Labs) to stain chromosomes or subjected to further processing for immunolocalisation. For immunolocalisation, prepared slides were air-dried and then heated in 10 mM citrate buffer pH 6 in an 850 W microwave for 45 s, taking care not to let the buffer boil. Slides were then immediately transferred to PBST (1× phosphate-buffered saline, 0.1% triton X100) for 10 min. Slides were blocked for 30 min at room temperature by applying 100 µl of 3% BSA (in PBST) to the surface of each slide using parafilm. Immunostaining was carried out using standard procedures described in Armstrong *et al.* (2002). Primary antibodies were used at the following dilutions in the blocking buffer: anti-*At*ASY1 guinea-pig or rabbit, 1 : 500 (Armstrong *et al.*, 2002); anti-*At*ZYP1 guinea-pig or rabbit, 1 : 500 (Higgins *et al.*, 2005; Osman *et al.*, 2018); anti-*Hv*HEI10 guinea-pig, 1 : 250 (Desjardins *et al.*, 2020); and anti-*Ta*CENH3, 1 : 200 (Osman *et al.*, 2021). Secondary antibodies were FITC (green) or Alexa Fluor 594 (red) conjugates (Sigma; Thermo Fisher, Waltham, MA, USA). Material for root tip analysis was generated by germinating seeds on moist filter paper at 20°C in the dark for 3 d. Roots were harvested when they were 1–3 cm long, fixed and used to prepare slides (as described above for anthers, except cellulase and pectolyase concentrations in the digestion mix were reduced to 0.15%). The viability of pollen grains was determined using Alexander staining (Alexander, 1969).

Microscopy

Fluorescence microscopy was carried out using a Nikon Eclipse 90i microscope fitted with a Nikon DS-Qi1Mc camera. NIS Elements software (Nikon) was used to capture images as Z-stacks with a 0.2 µM step. Mitotic chromosome, meiotic HEI10 foci and meiotic CENH3 signal counts were carried out using Z-stack images for accuracy. Stained pollen grains were viewed and imaged using a Motic BA310 digital microscope with an integrated 3MP camera and Motic Images Plus v.2.0 imaging software.

Virus-induced gene silencing

The Barley Stripe Mosaic Virus-mediated, VIGS system (BSMV VIGS; Yuan *et al.*, 2011; Desjardins *et al.*, 2020) was used to target expression of *TaFIGL1* in *T. aestivum* cultivar 'Bobwhite'. Two nonoverlapping regions with high predicted silencing efficiency were selected, following an *in silico* analysis of *TaFIGL1-A1* cds (*TraesCS5A02G109500*) with si-Fi21 (siRNA Finder, Lück *et al.*, 2019). For the first selected region, primers TaFIGL1-vigs-i_F 5′-AAGGAAGTTTAAAACTCAGCTTG CGAGAAGTTC-3′ and TaFIGL1-vigs-i_R 5′-AACCACCA CCACCGTCAGATAAGCAGGACGTGTG-3′ were used to amplify 439–708 bp of *TraesCS5A02G109500* coding region with Q5 DNA polymerase (NEB). For the second region, primers TaFIGL1-vigs-ii_F 5′-AAGGAAGTTTAAGATTCACT ACTATCTCAGCGC-3′ and TaFIGL1-vigs-ii_R 5′-AACCA CCACCACCGTAGATCCCGAGTAACCTTCTG-3′ were used to amplify 1537–1851 bp of *TraesCS5A02G109500* coding region with Q5 DNA polymerase (NEB). The amplicons were cloned into pCa-γbLIC to create a recombinant BSMV RNAγ. The recombinant pCa-γbLIC, as well as pCaBS-α and pCaBS-β, were then transformed into electrocompetent *Agrobacterium tumefaciens* (GV3101) and used to inoculate wheat plants Fnull (Desjardins *et al.*, 2020). For cytological analysis, anthers were dissected and fixed in 3 : 1 (v/v) ethanol: acetic acid at 14-d post-inoculation.

Skyfall × Cadenza hexaploid F3 marker-based recombination analysis

F_3 mapping populations fixed for either termination mutations (SxC_241; 74 lines) or WT alleles (SxC_123; 90 lines and SxC_322; 95 lines) at *FIGL1* homoeologues were developed to assess variation in marker-based recombination frequency. *Tafigl1* triple mutant (C0654 × C0900 × C2036) was crossed to Skyfall. F_1 plants were self-pollinated and F_2 siblings fixed for either WT or mutant alleles at the *FIGL1* homoeologues were selected and self-pollinated for F_3 seed. Lines of the F_3 populations were genotyped using the Axiom-35K Breeders array (Allen *et al.*, 2017) with genotype calling performed using the Axiom Analysis Suite (v.5.2.0.65) and prior model 'Axiom_WhtBrd-1.r4' and DQC cut-off of 0.8. Genotypes for probes with low call rates were manually confirmed before export. Physical positions and chromosome assignment were allocated to each marker by aligning to the IWGSC RefSeqv1.0 assembly (IWGSC, 2018) as described in Shorinola *et al.* (2022). Markers were filtered and removed if the parents were monomorphic, showed skewed segregation (heterozygous < 25% or > 75%), exceeded (> 20%) missing data limit, or markers were dominant (Allele A/B < 5). The remaining markers were allocated as either homozygous Cadenza (A), homozygous Skyfall (B), or segregating (X) and sorted by chromosome and physical position for each population. Markers showing segregation in any of the three populations were aligned (6475 markers) to enable the selection of 10 heterozygous intervals for genetic mapping (839 markers) to assess recombination frequency. All markers within the selected intervals were manually rescored to minimise errors and subsequent effects on genetic mapping. Genetic mapping was performed on each region individually using MSTmap online (http://www.mstmap.org/) with a LOD threshold of 8. After manual re-scoring and an initial round of mapping, additional markers were removed leaving 560 useful markers for the final mapping. For three regions (2A, 2B and 7B), the markers would not link for a complete linkage group for one of the populations and these regions were therefore manually split and re-mapped. The cM distance for each linkage group was used to determine the percentage difference in *figl1* (SxC_241) over *FIGL1* (mean of SxC_123 & SxC_322). As cM distances may become inflated due to erroneous data points leading to mis-mapping, the data, once sorted into genetic map order, was manually scored for each line as either having no COs, one CO, two or more COs or as miscall/mis-mapped. Real COs were described as where there was a change in allele score for at least three markers in a row, except for markers towards the end of a linkage group, where a single marker change was allowed. Furthermore, to be as inclusive as possible, each line was granted a single erroneous data point. The number of lines within each category was totalled for each region and calculated against the total number for the percentage of lines for each category. The difference between *figl1* and *FIGL1* populations was calculated. Analysing the percentage of lines that show no COs is potentially a more accurate way of assessing recombination as it will not be influenced by errors in the data and mis-mapping.

Statistics

HEI10 foci and seed count differences were tested for significance using a Mann–Whitney *U*-test; chiasma count differences using a pairwise Wilcoxon rank sum test and differences in pollen viability using a chi-squared contingency test. Mapping population differences were tested using ANOVA.

Results

FIGL1 is conserved in wheat

Wheat *FIGL1* orthologues were identified by Blast searches of publicly available wheat sequence databases using the Arabidopsis FIGL1 and rice FIGNL1 AA sequences as queries. Two *FIGL1* orthologues, *TtFIGL1-A1* (*TRITD5Av1G073320*) and *TtFIGL1-B1* (*TRITD5Bv1G056690*), were identified in tetraploid wheat, and three orthologues, *TaFIGL1-A1* (*TraesCS5A02G109500*), *TaFIGL1-B1* (*TraesCS5B02G110300*) and *TaFIGL1-D1* (*TraesCS5D02G123800*), in hexaploid wheat. All *FIGL1* orthologues were predicted to encode functional proteins of 688 AAs (Figs 1a, S1). FIGL1 is highly conserved between ploidy levels and homoeologues: the A homoeologues of the tetraploid and hexaploid species have identical predicted AA sequences, as do the B homoeologues, and the three hexaploid homoeologues, A, B and D, share 97% AA sequence identity, with polymorphisms at 21 of 688 residues (Fig. S1). A consensus sequence of the A, B and D FIGL1 homoeologues was used for

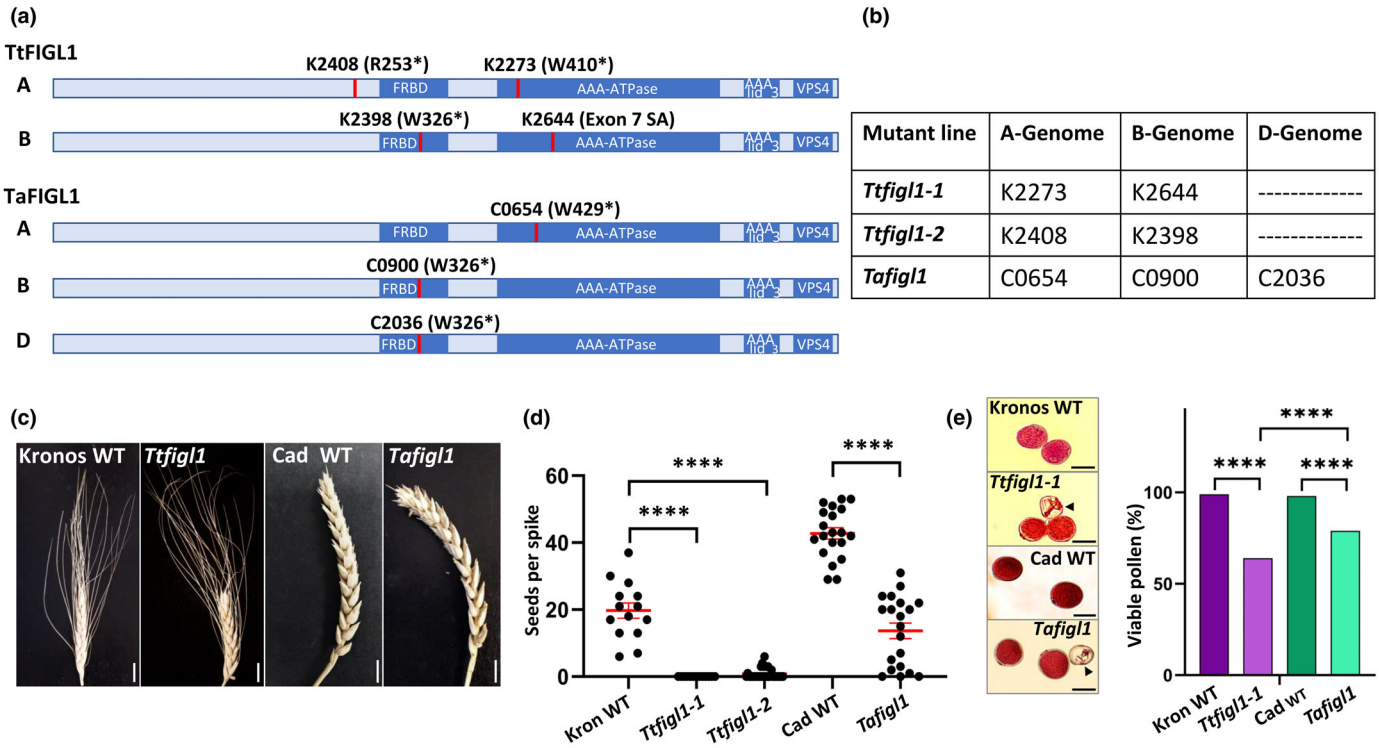

Mutant line	A-Genome	B-Genome	D-Genome
Ttfigl1-1	K2273	K2644	----------
Ttfigl1-2	K2408	K2398	----------
Tafigl1	C0654	C0900	C2036

Fig. 1 Fertility is reduced in wheat *figl1* mutants. (a) *TtFIGL1* and *TaFIGL1* coding region of homoeologues with conserved domains (dark blue boxes) and position/effect of EMS-induced mutations (red bars) indicated. Asterisks indicate a change to a premature termination codon, SA to splice-acceptor site variant. (b) Generation of double (tetraploid) and triple (hexaploid) mutant lines from single *figl1* mutants. (c) Comparison of spike morphology in wild-type (WT) and double or triple mutant lines (bars, 1 cm). (d) Scatter plot of seed counts per spike in *Ttfigl1-1*, *Ttfigl1-2* and *Tafigl1* compared with Kronos and Cadenza WTs respectively. Mean and SE bars are shown in red and asterisks indicate significance at the 0.0001% level ($n = 20$). (e) Alexander staining indicates reduced pollen viability in *Ttfigl1-1* and *Tafigl1* but is more extreme in the tetraploid than the hexaploid. Contents of viable grains stain red, inviable grains are shrunken and unstained (arrows); bars, 50 µm. Bar chart represents WT and mutant sample sizes of 280 for the tetraploid and 700 for the hexaploid. Asterisks indicate significance at the 0.0001% level.

comparison with other plant orthologues. Thus, wheat FIGL1 shares 78% overall AA sequence identity with rice FIGNL1 (541/696) and 57% with Arabidopsis FIGL1 (419/736; Fig. S2). These values rise to 90% (368/408) and 79% (322/408), respectively, in the C-terminal region of the protein (residues 280–688) where the predicted FRBD (FIGNL1 RAD51 Binding Domain; Yuan & Chen, 2013), AAA-ATPase, AAA_lid_3 and VPS4 conserved domains are located (Figs 1a, S2).

Fertility is reduced in *figl1* plants and differs between ploidies

Single homoeologue *figl1* mutants identified from the sequenced tetraploid Kronos EMS-induced population (Krasileva *et al.*, 2017) were crossed together to generate two independent double homozygote mutant lines, where A and B *FIGL1* homoeologues were both disrupted (*Ttfigl1-1* and *Ttfigl1-2*). Likewise, single homoeologue *figl1* mutants from the sequenced hexaploid Cadenza EMS-induced population (Krasileva *et al.*, 2017) were crossed to produce a triple homozygote mutant line, with A, B and D gene copies all disrupted (*Tafigl1*; Fig. 1b). All mutations generated premature termination codons, apart from one tetraploid B homoeologue splice-acceptor mutation, and all were located upstream (or just inside the upstream flank) of the C-terminal AAA-ATPase and VPS4 domain region so were predicted to be null mutations (Fig. 1a).

All three mutant lines showed normal vegetative growth and produced spikes of normal appearance (Fig. 1c). However, fertility was severely reduced in all cases, particularly in the tetraploid mutant. The WT tetraploid control, Kronos, had a mean seed count of 20 per spike ($n = 14$). By contrast, *Ttfigl1-1* was completely sterile and failed to produce any seeds from 13 spikes ($P < 0.0001$), while *Ttfigl1-2* produced a total of 16 seeds from 34 spikes ($P < 0.0001$) with only five spikes containing any seeds at all (maximum number per spike was 6; Fig. 1d). Seed count was also reduced in *Tafigl1* (mean = 14 ± 2.3 per spike vs 43 ± 1.7 in WT Cadenza, $n = 20$ (the first 5 spikes from 4 plants), $P < 0.0001$) but varied between spikes, ranging from 0 to 31 seeds per spike compared with 29–53 in WT (Fig. 1d). Thus, although some spikes produced no mature seeds (but often contained tiny, aborted seeds), others, even within the same plant, contained up to 72% of the WT mean seed number.

Pollen grain staining in the tetraploid, *Ttfigl1-1*, indicated that 36% were inviable compared with only 1% in WT Kronos ($\chi^2_{(1)} = 111.9$, $P < 0.0001$, $n = 280$), whereas in the hexaploid, *Tafigl1*, 21% of grains were inviable compared with 2% in WT Cadenza ($\chi^2_{(1)} = 130.3$, $P < 0.0001$, $n = 700$; Fig. 1e). This suggested that defects in gamete formation hampered seed

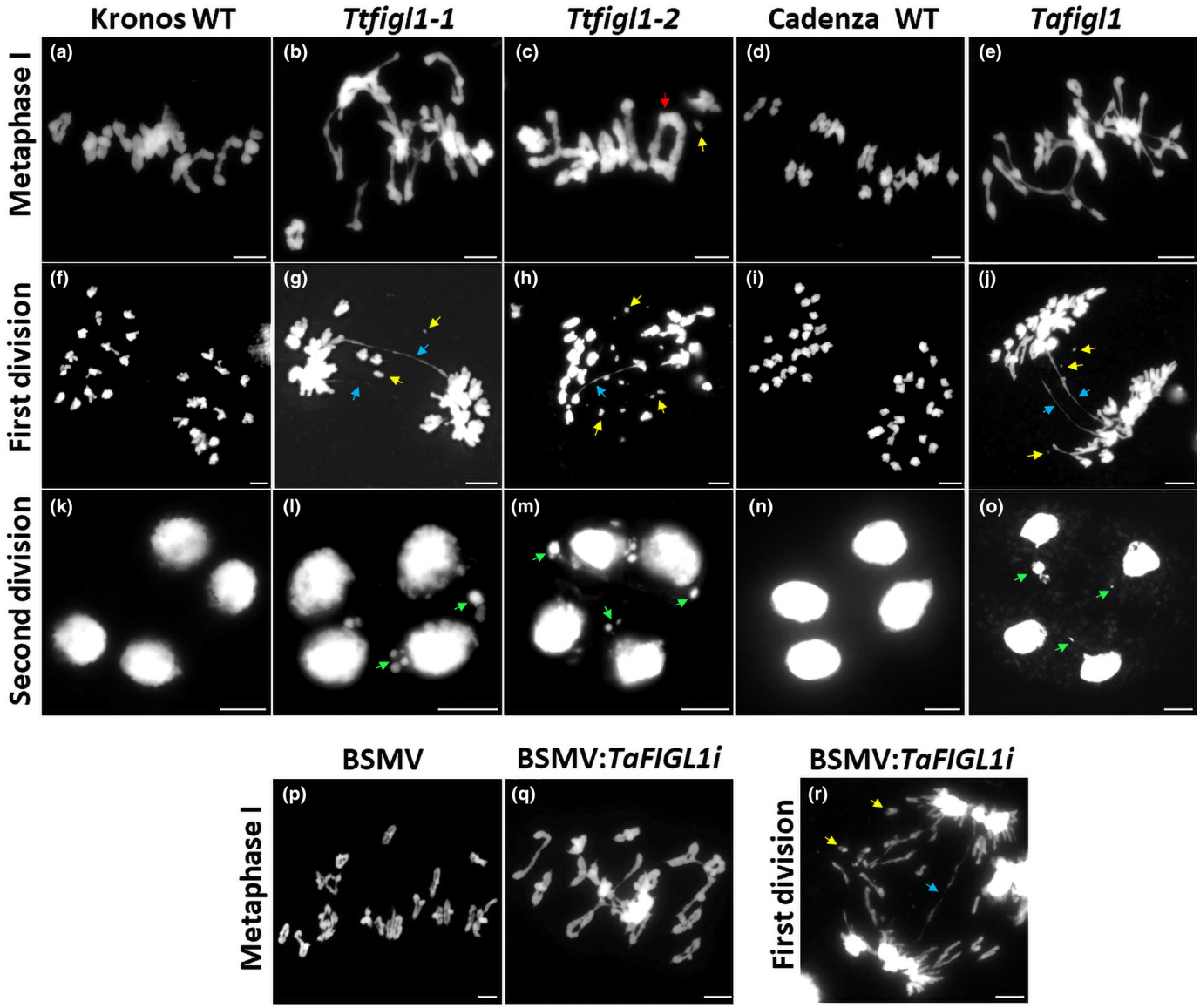

Fig. 2 Disruption of wheat *FIGL1* results in abnormal chromosome associations and fragmentation. Chromosome spreads of pollen mother cells (PMCs) from double tetraploid and triple hexaploid *figl1* mutants and their wild-type (WT) controls at metaphase I (a–e), the first meiotic division (f–j) and following the second meiotic division at the tetrad stage (k–o). Arrows indicate a quadrivalent structure (red), example fragments (yellow), chromosome bridges at the first division (blue) and stray chromatin at the tetrad stage (green). (p–r) Virus-induced gene silencing (VIGS) knockdown of *FIGL1* in the hexaploid Bobwhite showing the empty vector control at metaphase I (p), the knockdown line with abnormal chromosome associations at metaphase I (q) and with chromosome bridges and fragments at the first division (r). DNA is stained with 4′,6′-diamidino-2-phenylindole (DAPI). Bars, 10 µm.

development in *figl1* of both ploidies but the tetraploid appeared more severely affected than the hexaploid ($\chi^2_{(1)} = 21.5$, $P < 0.0001$), consistent with their relative reduction in seed production.

FIGL1 disruption results in aberrant chromosome associations and chromosome fragmentation

To investigate the basis of reduced pollen viability and fertility in *figl1* mutants, we carried out a cytological analysis of pollen mother cells (PMCs) of *Ttfigl1-1*, *Ttfigl1-2* and *Tafigl1* compared with WT. During meiotic prophase I, pairing and recombination of homologous chromosomes in the tetraploid WT leads to the appearance of 14 bivalent structures at metaphase I, with homologues held together by chiasmata, the cytological manifestation of COs (Fig. 2a). This is followed by separation of the homologues at anaphase I and segregation into two cohorts of 14 chromosomes (Fig. 2f). At metaphase I in *Ttfigl1-1* and *Ttfigl1-2* abnormal interbivalent associations, multivalent structures and, more rarely, chromosome fragments were apparent (Fig. 2b,c). As chromosomes separated at the first meiotic division, chromosome bridges and more extensive fragmentation were observed

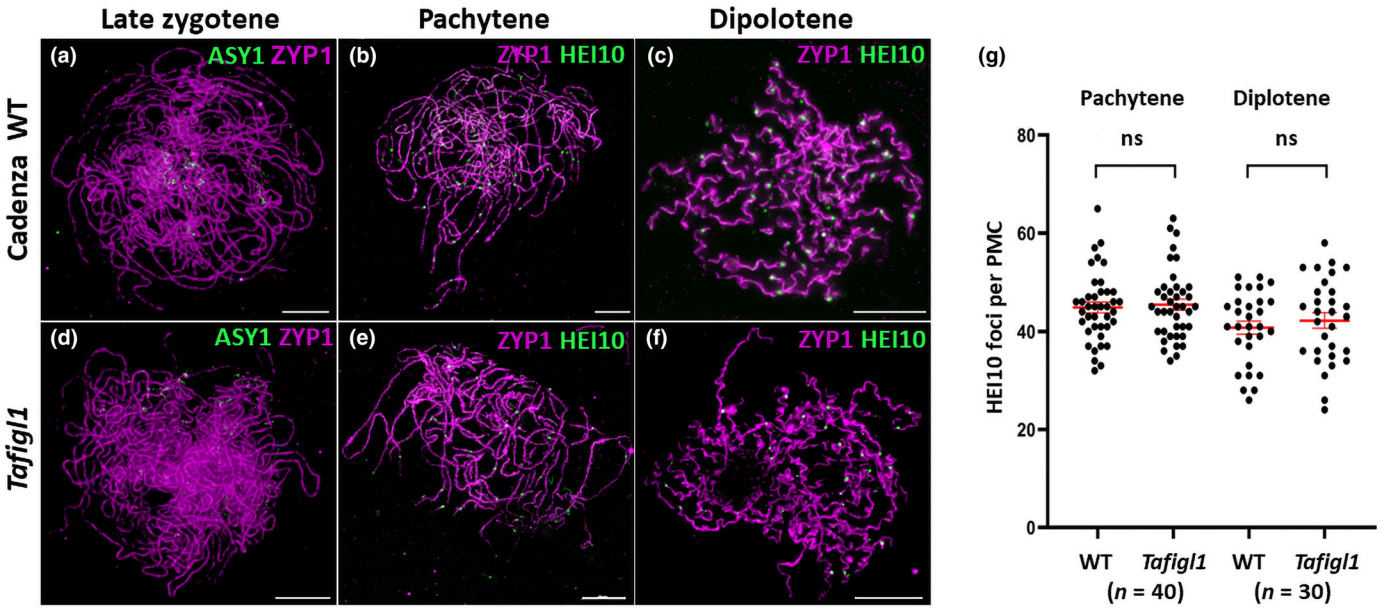

Fig. 3 Assessment of class I crossover (CO) frequency in hexaploid wheat *figl1*. (a–f) Dual immunolocalisation of pollen mother cells (PMCs) from *Tafigl1* and its wild-type (WT) control at late prophase I: (a, d) ASY1 (green), ZYP1 (magenta) at late zygotene; (b, e) ZYP1 (magenta), HEI10 (green) at pachytene and (c, f) ZYP1 (magenta), HEI10 (green) at diplotene. (g) Scatterplot of HEI10 foci counts per PMC at pachytene or diplotene with mean and SE bars shown in red and ns indicating statistical nonsignificance. Bars, 10 µm.

(Fig. 2g,h; 86% of *Ttfigl1-1* PMCs at first division had bridges and/or fragmentation, $n = 56$). A similar phenotype was observed in *Tafigl1* (Fig. 2e,j), where 95% ($n = 63$) of PMCs exhibited chromosome bridges and/or fragments at the first division, rather than forming 21 discrete bivalents and segregating normally, as in the hexaploid WT (Fig. 2d,i). Following the second meiotic division, abnormal tetrads with stray chromatin or unbalanced or micro/poly-nuclei were observed in *Ttfigl1* and *Tafigl1* (Figs 2k–o, S3), consistent with the reduced fertility of these lines.

Because lines derived from the EMS-induced populations have a high background mutational load (Uauy *et al.*, 2017), we independently silenced the *TaFIGL1* gene in hexaploid wheat (Bobwhite) using BMSV VIGS to confirm that the cytological phenotype of the EMS-induced mutant lines was due to disruption of *FIGL1*. Plants infected with the BSMV:*TaFIGL1-i* construct exhibited abnormal chromosome associations at metaphase I, and 66% ($n = 32$) of PMCs at the first division contained chromosome bridges and/or fragments (Fig. 2q,r). By contrast, PMCs from control plants infected with the empty virus produced normal discrete bivalents at metaphase I (Fig. 2p). The similarity in cytological phenotype between the VIGS-treated line and the *Ttfigl1-1*, *Ttfigl1-2* and *Tafigl1* EMS-induced mutant lines thus confirms the wheat *figl1* phenotype.

The unexpected finding that *Tafigl1* retained a modest level of fertility, despite exhibiting similar cytological defects to *Ttfigl1-1* (and with a higher proportion of affected first-division nuclei), prompted us to examine the next generation. Seeds from selfed *Tafigl1* were viable (100% seed germination, $n = 30$), producing plants with the parental phenotype of abnormal interbivalent associations at metaphase I, chromosome bridges and fragments at anaphase I and abnormal tetrads (Fig. S4a). Similar to *Tafigl1*, they also went on to produce seeds at a reduced level (0–30 seeds per spike). We also checked for the possibility of aneuploidy amongst the progeny. Chromosome number was difficult to assess directly due to the extensive meiotic chromosome associations, so we used two indirect approaches. First, we counted chromosomes in Z-stack images of mitotic root tip nuclei at prometaphase. This revealed the normal number of 42 chromosomes per nucleus ($n = 5$; Fig. S4b). Second, we carried out dual localisation of ZYP1 and CENH3 in late pachytene PMCs when chromosomes are expected to be fully paired and synapsed (to be described later). In four of the five plants examined, this revealed the presence of 21 pairs of CENH3 signals associated with linear ZYP1 signal, confirming that nuclei contained the correct number of chromosomes which could pair and synapse apparently normally (Fig. S4c). The remaining plant appeared to contain one 'extra' chromosome, forming 21 pairs of CENH3 signals plus an additional single signal (Fig. S4d). Thus, as far as we could tell, most progeny possessed an identical phenotype to the parent, with only a minority showing evidence of aneuploidy.

FIGL1 limits class II crossover formation

Next, we investigated the effect of *FIGL1* disruption on recombination. It was not possible to carry out meaningful chiasma counts in the *figl1* EMS-induced mutants due to the extensive metaphase I chromosome associations. We therefore assessed CO

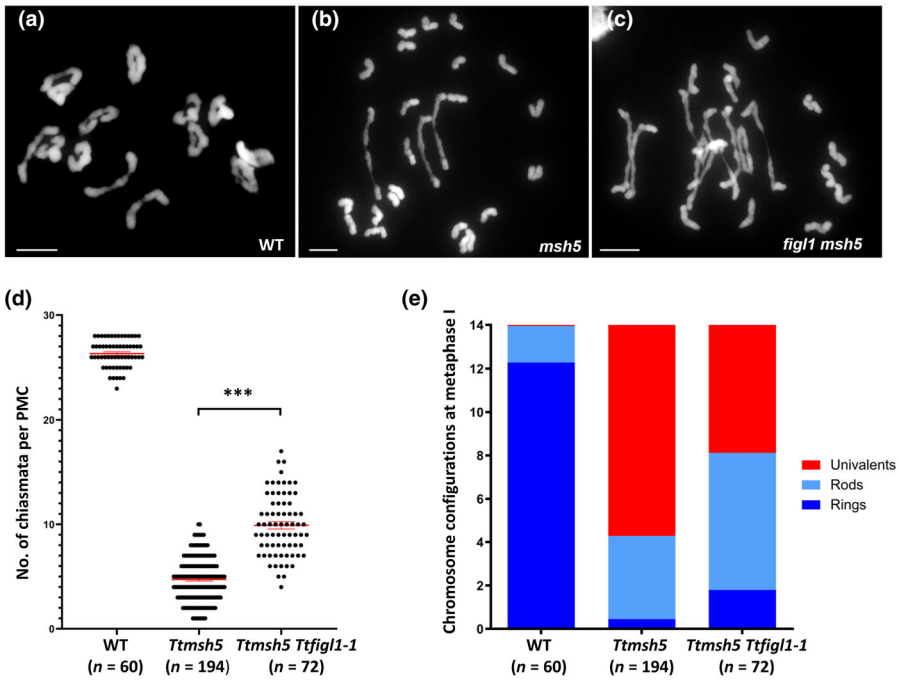

Fig. 4 Assessment of chiasma frequency in a tetraploid wheat *figl1-1 msh5* quadruple mutant. Chromosome spreads of (a) Kronos wild-type (WT), (b) *Ttmsh5* and (c) *Ttfigl1-1 Ttmsh5* at metaphase I. (d) Scatterplot of chiasma frequency per pollen mother cell (PMC) with mean and SE bars shown in red and asterisks indicating statistical significance at the 0.001 level. (e) Mean proportion of rod bivalents, ring bivalents and univalents per PMC. DNA is stained with 4′,6′-diamidino-2-phenylindole (DAPI); bars, 10 µm.

formation in *Tafigl1* using immunolocalisation of HEI10 (Chelysheva *et al.*, 2012), which is routinely used as a marker of class I CO sites at late prophase I in plants (Chelysheva *et al.*, 2012; Wang *et al.*, 2012; Hesse *et al.*, 2019; Desjardins *et al.*, 2020; Osman *et al.*, 2021). First, we examined chromosome synapsis in *Tafigl1* by carrying out dual immunolocalisation of ASY1, which marks the unsynapsed chromosome axes (Armstrong *et al.*, 2002), and the SC transverse filament protein, ZYP1 (Higgins *et al.*, 2005). By late prophase I, linear ZYP1 signal had largely replaced ASY1 signal along the paired chromosomes in WT PMCs, with just a few traces of ASY1 signal remaining (Fig. 3a). A similar pattern of ZYP1 staining was observed in *Tafigl1* at late prophase I, confirming the ability of the mutant to pair and synapse, and indicating that wheat FIGL1 is dispensable for this process (Fig. 3d). We then used dual immunolocalisation of ZYP1 and HEI10 at late prophase I to estimate class I CO frequency. HEI10 foci were counted at two stages: late pachytene, when ZYP1 was fully linear throughout the nucleus and HEI10 formed large foci (Fig. 3b,e), and slightly later, in early diplotene, when ZYP1 remained staining the chromosomes which displayed a 'corkscrew-like' morphology (a distinctive feature of wheat hexaploid chromosomes at this stage; Fig. 3c,f). At both stages, the number of HEI10 foci in *Tafigl1* and WT was not significantly different (mean foci per PMC at pachytene in *Tafigl1* = 45.4 ± 7.1 vs 44.9 in WT, $n = 40$, $P = 0.79$; mean foci per PMC at diplotene in *Tafigl1* = 42.2 ± 8.6 vs 40.8 ± 7.4 in WT, $n = 30$, $P = 0.52$; Fig. 3g). This indicates that mutation of *FIGL1* has no obvious effect on the formation of class I COs.

We then made use of a tetraploid double homozygote *msh5* mutant defective in class I CO formation (Desjardins *et al.*, 2020) to genetically investigate class II CO formation in wheat *figl1*. The *Ttmsh5* mutant was crossed with *Ttfigl1-1* to generate the quadruple mutant *Ttfigl1-1 Ttmsh5*, to determine whether mutation of *FIGL1* could restore COs in *Ttmsh5*. Mean chiasma frequency in the WT tetraploid, Kronos, was 26.4 ± 0.17 (Fig. 4a,d), whereas in *Ttmsh5*, it was 4.7 ± 0.15 ($n = 194$), compared with 9.9 ± 0.34 ($n = 72$) in *Ttfigl1-1 Ttmsh5* ($P < 0.001$; Fig. 4b–d). We also observed a corresponding increase in rod and ring bivalents, and a decrease in univalent pairs in the quadruple mutant relative to *Ttmsh5* (Fig. 4e). The rescued chiasmata were randomly distributed around the mean and chiasma frequency did not differ significantly from a Poisson-predicted distribution ($\chi^2_{(25)} = 9.9$, $n = 72$, $P > 0.05$). This indicates that mutation of *figl1* can partially rescue the *zmm* phenotype of *msh5* in wheat and implies that the additional chiasmata were formed via the class II pathway. Taken together, the cytological data suggest that wheat FIGL1 has no discernible effect on the formation of class I COs, but limits class II COs.

Genetic mapping reveals changes in the recombination pattern of *figl1* mutants

The moderate fertility of *Tafigl1* meant that *FIGL1* disruption had potential utility for breeding, so it was of interest to carry out recombination mapping in this line, especially as the tetraploid data indicated that disruption of *FIGL1* increased class II COs. Molecular marker-based analysis and genetic mapping were performed on hexaploid F_3 populations fixed for either null mutations or WT alleles at *FIGL1*, as an alternative method of measuring effects on recombination frequency (Fig. 5a). In total, 13 intervals were analysed on 8 chromosomes. Distances based on genetic mapping (cM) were compared for each region between the populations, with eight regions showing increased recombination (> 10%), three regions showing no effect

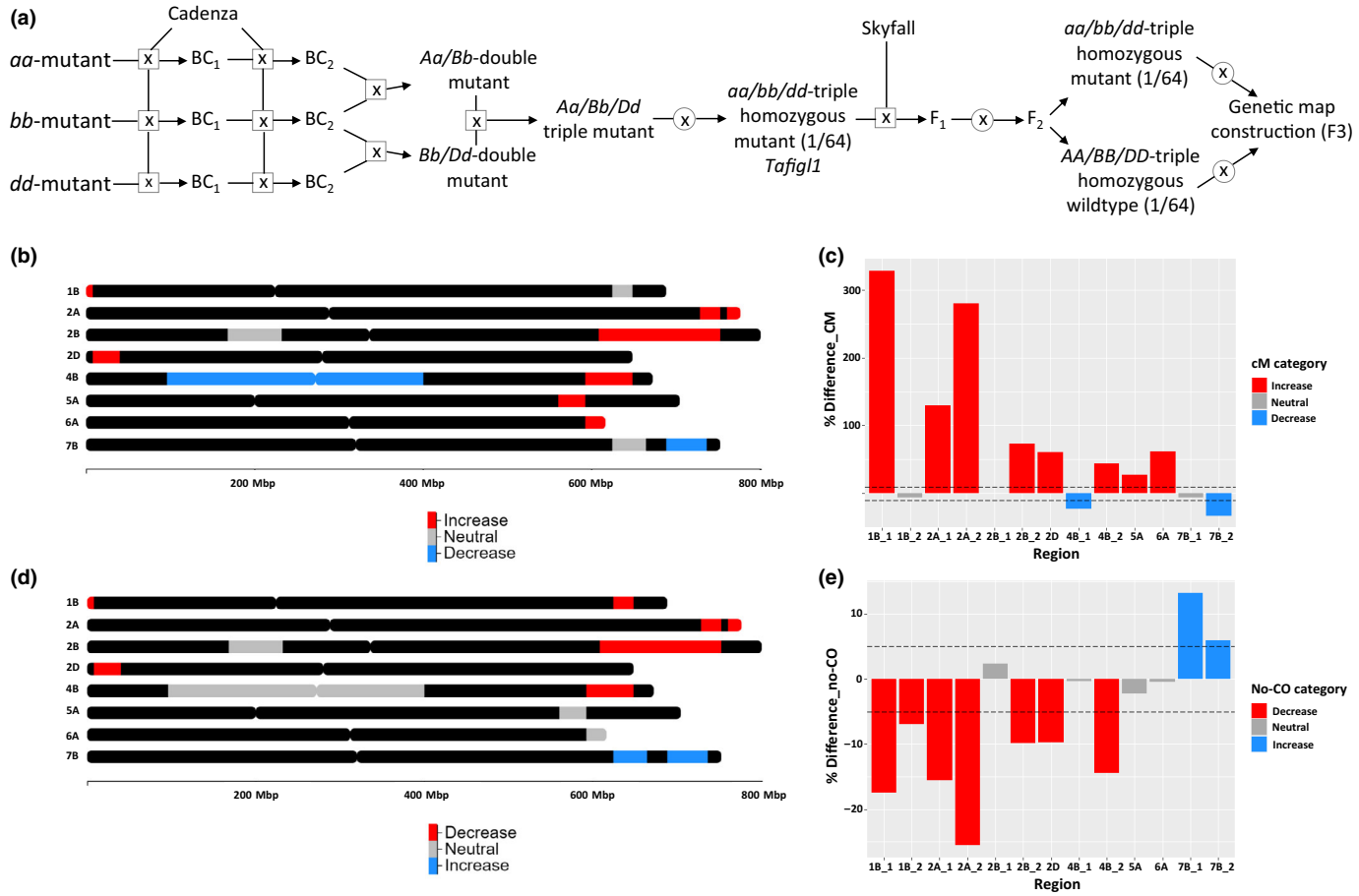

Fig. 5 Generation of a hexaploid wheat triple *figl1* mutant and F_3 mapping populations for genetic marker-based recombination analysis. (a) Crossing scheme for generating the triple mutant *Tafigl1* (background Cadenza) and the Skyfall × Cadenza F_3 mapping populations fixed at *FIGL1* for either wild-type (*AA/BB/DD*) or mutant (*aa/bb/dd*) alleles. (b, d) Chromosome depictions showing the locations of the 13 regions and effects as analysed by cM distance from genetic mapping (b) or lines with no crossovers (d). Regions are aligned and ordered by IWGSC RefSeqv1.0 coordinates (Mbp). Beneficial effects from the *figl1* triple mutant population are highlighted in red, neutral regions in grey and detrimental effects in blue. (c, e) Bar charts showing the % differences between *figl1/FIGL1* populations ordered by chromosome region. Bars are coloured by designated effect – note that red corresponds to an increase in recombination in each case. Dashed lines represent an increase/decrease of 10% in (c) and 5% in (e).

(±10%) and two regions showing decreased recombination (> −10%; Tables 1a, S3; Fig. 5b,c). There was no overall statistical increase in cM distance across intervals ($P = 0.17$), despite there being an average 52% increase in distance across intervals. This was mostly due to intervals 1B_1, 2A_1 and 2A_2 exhibiting large (> 100%) expansion in the genetic map (Tables 1a, S3; Fig. 5b,c).

To confirm these effects on recombination, and nullify any potential errors from mis-mapping, we also analysed the data by manually scoring the genotype data for lines showing no COs (Table 1b; Fig. 5d,e). Using this method, we compared the percentage of lines from *figl1/FIGL1* populations showing no recombination. We discovered that 7 of the 13 intervals had fewer lines showing no COs (> −5%), 4 regions showed no effect (±5%) and 2 were increased (> 5%). Across all regions, there were 6% fewer NCO lines in the *figl1* null mutant population although, again, this was not statistically significant ($P = 0.33$). These results suggest that *figl1* null mutants do not perturb recombination frequency universally but do impact intervals on some chromosomes.

Discussion

We investigated genetic disruption of the conserved AAA-ATPase FIGL1 as a potential strategy for modifying meiotic recombination in wheat, where the generation of new allelic combinations through plant breeding is laborious and time-consuming, particularly in hexaploid (bread wheat) varieties.

Cytological analysis of wheat *figl1* tetraploid double and hexaploid triple mutants, and *FIGL1* VIGS knockdown lines, revealed an identical phenotype of abnormal interbivalent chromosome associations at metaphase I, followed by chromosome bridges and fragmentation as homologues separated at anaphase I. Wheat *figl1* mutants appeared to undergo normal and full synapsis implying that the interbivalent associations at metaphase I were between non-homologous chromosomes. One possibility

Table 1 Variation in hexaploid wheat recombination for the 13 selected segregating regions calculated by either the cM mapping distance (a) or the proportion of lines showing no crossovers (b).

(a)			cM Distance					
Chromosome	Region_35K SNPId	Region (IWGSC_v1)	*figl_1*	FIGL_1	Delta	% Difference	Category (%)	Effect
1B_1	AX-95106318–AX-94762873	464 660–4346 060	30.0	7.0	23.0	328	> 10	Increase
1B_2	AX-94395727–AX-94534843	629 486 741–646 169 513	29.2	31.2	−1.9	−6	±10	Neutral
2A_1	AX-94396447–AX-94607578	734 346 580–759 732 403	82.7	35.9	46.8	130	> 10	Increase
2A_2	AX-94881482–AX-95631542	762 292 250–775 523 929	39.6	10.4	29.2	281	> 10	Increase
2B_1	AX-94560891–AX-94576276	174 592 316–227 080 955	12.5	12.5	0.1	1	±10	Neutral
2B_2	AX-94426498–AX-94936841	610 916 709–750 015 686	122.0	70.3	51.7	74	> 10	Increase
2D	AX-94391187–AX-94806590	12 885 312–36 434 280	37.7	23.4	14.3	61	> 10	Increase
4B_1	AX-94427138–AX-94980498	96 192 786–394 603 091	5.8	7.6	−1.8	−23	> −10	Decrease
4B_2	AX-94528470–AX-95084128	595 269 295–643 651 032	41.1	28.5	12.6	44	> 10	Increase
5A	AX-94383503–AX-95002541	569 463 745–588 874 315	22.1	17.4	4.7	27	> 10	Increase
6A	AX-94461279–AX-94917451	596 911 786–617 658 214	75.8	46.9	28.9	62	> 10	Increase
7B_1	AX-94634240–AX-94467701	625 883 960–657 934 272	25.2	26.9	−1.7	−6	±10	Neutral
7B_2	AX-95175600–AX-94467581	693 169 401–730 909 860	32.9	49.0	−16.1	−33	> −10	Decrease
		Mean all regions	42.8	28.2	14.6	52^{ns}		

(b)			Lines showing No-CO				
Chromosome	Region_35K SNPId	Region (IWGSC_v1)	*figl_1* (%)	FIGL_1 (%)	Delta (%)	Category (%)	Effect
1B_1	AX-95106318–AX-94762873	464 660–4346 060	74	92	−17	> −5	Decrease
1B_2	AX-94395727–AX-94534843	629 486 741–646 169 513	65	72	−7	> −5	Decrease
2A_1	AX-94396447–AX-94607578	734 346 580–759 732 403	46	62	−16	> −5	Decrease
2A_2	AX-94881482–AX-95631542	762 292 250–775 523 929	62	88	−25	> −5	Decrease
2B_1	AX-94560891–AX-94576276	174 592 316–227 080 955	88	85	2	±5	Neutral
2B_2	AX-94426498–AX-94936841	610 916 709–750 015 686	38	48	−10	> −5	Decrease
2D	AX-94391187–AX-94806590	12 885 312–36 434 280	59	69	−10	> −5	Decrease
4B_1	AX-94427138–AX-94980498	96 192 786–394 603 091	91	91	0	±5	Neutral
4B_2	AX-94528470–AX-95084128	595 269 295–643 651 032	50	64	−14	> −5	Decrease
5A	AX-94383503–AX-95002541	569 463 745–588 874 315	78	81	−2	±5	Neutral
6A	AX-94461279–AX-94917451	596 911 786–617 658 214	54	54	0	±5	Neutral
7B_1	AX-94634240–AX-94467701	625 883 960–657 934 272	78	65	13	> 5	Increase
7B_2	AX-95175600–AX-94467581	693 169 401–730 909 860	54	48	6	> 5	Increase
		Mean all regions	64.4	70.7	-6^{ns}		

The percentage difference was calculated for each analysis, and each region was categorised by its percentage difference as resulting in either, increasing, neutral or decreased recombination. For analysis of cM distance, the following categories were designated: Increasing (> 10%); Neutral (±10%); Decreasing (> −10%), and for the No-CO analyses: Increasing (> 5%); Neutral (±5%); Decreasing (> −5%). Note that a decrease in No-COs corresponds to an increase in recombination. ns, nonsignificance.

is that they were simply due to chromosome entanglements or interlocks which failed to be corrected, thus giving rise to chromosome bridges at the division stages. Alternatively, interbivalent associations may have been caused by aberrant recombination events, either between homologous sites on homoeologous chromosomes or between ectopic sites. Left unresolved, these would also lead to anaphase I bridges (as indeed would unrepaired/unresolved recombination intermediates between homologous chromosomes, although these would not be apparent at metaphase I). Yet, a third possibility is that chromosome associations arose from defects left over from meiotic S-phase, and in this context, it is worth noting that there have been recent reports of a role for mammalian FIGNL1 in DNA replication (Ito *et al.*, 2023; Q. Zhang *et al.*, 2023), although to date, there is no evidence for such a role in plants. Similar abnormal chromosome associations occur in rice *fignl1* mutants and have been reported to be non-homologous (Zhang *et al.*, 2017; Yang *et al.*, 2022). In Arabidopsis and rice, FIGL1/FIGNL1 acts downstream of DSBs at the strand invasion step of recombination, such that the chromosome associations observed in rice *fignl1* are P31^{comet}-dependent (Girard *et al.*, 2015; Ji *et al.*, 2016; Yang *et al.*, 2022). It therefore seems likely that wheat *figl1* chromosome associations are similarly recombination-dependent and represent a form of interaction which has failed to be repaired or resolved before the division stages. However, further study would be required to confirm this and to determine the type of interaction(s) involved.

Given the severe cytological phenotype of rice *fignl1* PMCs, it is perhaps unsurprising that pollen was inviable and mutant plants were sterile (Zhang *et al.*, 2017). *FIGL1* disruption in other distantly related diploid crops (pea and tomato) also led to sterility, although the cytological basis of this was not reported (Mieulet *et al.*, 2018). Similarly, wheat tetraploid double *figl1* mutants were almost completely sterile and produced very few seeds. By contrast, the hexaploid triple mutant retained a

reasonable level of fertility, with individual spikes producing up to 72% of the WT mean number of seeds, despite having a similar abnormal cytological phenotype to the tetraploid wheat double and rice mutants. One possible explanation for this is that the hexaploid mutant is more tolerant of chromosome damage than the tetraploid and diploids, possessing three sub-genomes and therefore a greater chance of segregating a viable complement of chromosomes to at least some of its haploid microspores. Consistent with this interpretation, 36% of pollen in the tetraploid was inviable compared with only 21% in the hexaploid, despite the hexaploid having a higher proportion of cytologically aberrant first-division nuclei (95% compared to 86%). Presumably, any such hexaploid resilience might also be advantageous during the subsequent stages of fertilisation and seed development, which may explain the difference in fertility between the two ploidies. It is also possible that genetic background differences over and above chromosome copy number *per se* may have contributed to *Tafigl1* having a higher fertility than *Ttfigl1-1 or Ttfigl1-2*.

Despite the overall moderate level of fertility in the hexaploid, there was wide variation in the number of seeds per spike (0–31). However, even in the WT there was considerable variation (29–53 seeds, representing a range of 24), possibly because the process of pollination, fertilisation etc. is somewhat stochastic in nature. The proportion of viable pollen in the hexaploid was relatively high (*c.* 80%). Nevertheless, some of the grains may have contained defects affecting their ability to support normal fertilisation or seed development, either resulting from *FIGL1* disruption or, indeed, from other EMS-induced background mutations and this, together with the (currently unexplored) effects of *FIGL1* disruption in female meiosis, may have contributed to the increased variability of individual spike seed counts in the mutant compared with the WT. This is consistent with the observation of tiny, aborted seeds in some of the *Tafigl1* spikes. Seeds that did make it through to maturity were viable and produced plants of normal appearance with a similar *figl1*-like cytological phenotype and fertility to the parental line and, although we did observe one example of aneuploidy (one extra chromosome), this phenomenon did not appear to be widespread and is unlikely to preclude the use of *FIGL1* disruption for breeding purposes.

To determine whether *FIGL1* disruption might be useful for plant breeding, we investigated its effects on recombination. We found no evidence that *figl1* mutation had any effect on class I CO frequency, such that HEI10 foci numbers in the triple mutant, *Tafigl1*, in late prophase I did not differ significantly from WT. As it was not feasible to investigate class II COs directly in the hexaploid using a *figl1 zmm* sextuple mutant, we assessed them in the tetraploid by creating a *figl1-1 msh5* quadruple mutant. This revealed a 2.1-fold increase in the frequency of chiasmata per meiosis, from 4.7 to 9.9, in *figl1-1 msh5* compared with a *msh5* (class I) double mutant. Rescued chiasmata were randomly distributed around the mean and their frequency did not differ significantly from a Poisson-predicted distribution, as would be expected for class II COs (Higgins *et al.*, 2004, 2008a, b; Desjardins *et al.*, 2020). These results are consistent with data from Arabidopsis and rice, where FIGL1 also limits class II COs but does not affect class I COs (Girard *et al.*, 2015; Yang *et al.*, 2022).

Genetic mapping in the hexaploid was performed using Skyfall × Cadenza mapping populations and involved 13 marker intervals across eight different chromosomes. There was no overall statistical increase in recombination based on cM distance, despite a mean interval increase of 52%. However, three of the intervals, 1B_1, 2A_1 and 2A_2, were associated with very large increases in map distance (100–300%), indicating local changes in the recombination landscape. Furthermore, genotypic analysis to identify lines with no-COs largely corroborated the mapping data, indicating that seven intervals showed an increase in recombination (i.e. had fewer no-COs) including 1B_1, 2A_1 and 2A_2. Three intervals, 4B_1, 7B_1 and 7B_2, showed a decrease in recombination. Of these, 4B_1 is a large interval spanning the centromeric region where recombination rates are low (Saintenac *et al.*, 2009; Choulet *et al.*, 2014) so data for this region are based on a relatively small number of plants (Table S3) and the apparent decrease in recombination was indicated only by the cM distance data; the no-CO data (which is a potentially more accurate method of assessment – see the Materials and Methods section) indicated no change in recombination. The decrease in recombination on chromosome 7B appears more compelling, involving two intervals indicated by the no-CO method, one of which was also indicated by the cM distance data.

The origin of the increased COs in some intervals is unknown but it seems likely they arose through the class II pathway, given that the frequency of HEI10 foci was unchanged in the hexaploid mutant, class II COs were increased in the tetraploid mutant and *FIGL1/FIGNL1* disruption is known to increase class II COs in other plants (Girard *et al.*, 2015; Yang *et al.*, 2022). Notably, intervals 1B_1, 2A_1 and 2A_2, which showed the highest levels of recombination were all distally located, which is consistent with previous studies of plant anti-recombinases. Uneven increases in COs were observed in Arabidopsis *figl1* mutants, where the biggest increases were also in the distal regions (Girard *et al.*, 2015), while in the Poaceae, recombination increases due to mutation of *RECQL4* mutation in barley and *FANCM* in hexaploid wheat were similarly distally skewed (Arrieta *et al.*, 2021; Desjardins *et al.*, 2022). It therefore appears that the recombination landscape of anti-recombinase mutants is influenced by similar factors which affect WT recombination such that they tend to occur at the gene-rich, sub-telomeric regions of the chromosomes (Higgins *et al.*, 2012; Osman *et al.*, 2021).

The reason for the reduction in recombination on chromosome 7B is currently unclear. Possibly, it may reflect a more random distribution of COs, which might be expected to result from an increase in class II COs. Alternatively, a reduction in class I COs in this region (and increase in other regions) could imply a redistribution of class I COs and, while we cannot rule out this interpretation, it would be unexpected and we currently have no other evidence to support it. Equally, we are currently unaware of any additional factors that could account for the decrease in recombination in 7B.

This study adds to an increasing body of evidence that disruption of *FIGL1/FIGNL1* can have distinct outcomes in different

plant species. The presence of unresolved chromosome associations in wheat and rice and their absence from *Arabidopsis* and maize *figl1/fignl1* mutants implies no simple relationship with either ploidy or genome size. In fact, genetic analysis in *Arabidopsis* and maize has revealed a complex interplay between FIGL1 and BRCA2, whereby FIGL1 acts as a negative regulator in Arabidopsis HR, antagonising BRCA2 to control RAD51 and DMC1 focus formation (Kumar *et al.*, 2019), and as a positive regulator of recombination in maize, acting co-ordinately with dosage-sensitive BRCA2 (T. Zhang *et al.*, 2023). Notably, the maize *figl1 brca2* double mutant has an identical cytological phenotype to wheat and rice *figl1/fignl1* mutants, displaying abnormal chromosome associations at metaphase I and bridges/fragmentation at anaphase I (T. Zhang *et al.*, 2023). It would therefore be interesting to investigate the relationship between *FIGL1* and other recombination proteins in future wheat studies.

To the best of our knowledge, this is the first study of *FIGL1* in a polyploid plant and increases our understanding of recombination in crop species. The discovery that similar cytological abnormalities could impact fertility differently in the tetraploid double and hexaploid triple mutants was unexpected and suggests that the extra ploidy level may afford a degree of resilience to chromatin damage. This could have important implications for other recombination-modification strategies. The modest fertility of the hexaploid triple mutant and the perturbation of recombination observed in some mapping intervals, despite examining only a limited number of regions, suggests that *FIGL1* disruption may be a useful addition to the plant breeding toolkit. The large increases in recombination frequency observed in some intervals could help to speed up the breeding of desired haplotypes, which typically involves screening large populations of plants over many generations, thus reducing time and cost. Perturbation of recombination might also help to reveal inaccessible, potentially useful, genetic variation and disrupt blocks of linkage disequilibrium, freeing agronomically beneficial traits from linked, undesirable ones.

Acknowledgements

This work was funded by UKRI through a BBSRC strategic Long and Large grant (sLoLa), BB/N002628/1. We would like to thank Helen Harper as sLoLa project coordinator, Mark Winfield for helpful discussions and support (both from the University of Bristol, UK), the sLoLa Steering Committee for advice throughout the project and Chris Burt (RAGT) and Nickolas Bird (KWS) for their support of the sLoLa project. Thanks also go to Stefan Heckmann (IPK, Gatersleben, Germany) for the kind gift of anti-HvHEI10 antibody.

Competing interests

None declared.

Author contributions

KO, SDD, FCHF, ESM, JDH, KJE, CU and IRH designed the research. KO, SDD, JS, AJB, KJE and KK performed the experiments. KO, SDD, JS, CU, AJB, KJE, JDH, FCHF and ESM analysed the data. KO, SDD, JS, CU and FCHF wrote the manuscript. All authors read and corrected the manuscript. KO and SDD contributed equally to this work.

ORCID

James D. Higgins https://orcid.org/0000-0001-6027-8678
Kostya Kanyuka https://orcid.org/0000-0001-6324-4123
Kim Osman https://orcid.org/0000-0002-0282-4148
Eugenio Sanchez-Moran https://orcid.org/0000-0002-7417-0024
Cristobal Uauy https://orcid.org/0000-0002-9814-1770

Data availability

The data that support the findings of this study are available in the Supporting Information of this article.

References

Adamski NM, Simmonds J, Brinton JF, Backhaus AE, Chen Y, Smedley M, Hayta S, Florio T, Crane P, Scott P *et al.* 2021. Ectopic expression of *Triticum polonicum* VRT-A2 underlies elongated glumes and grains in hexaploid wheat in a dosage-dependent manner. *Plant Cell* **33**: 2296–2319.

Alexander MP. 1969. Differential staining of aborted and nonaborted pollen. *Stain Technology* **44**: 117–122.

Allen AM, Winfield MO, Burridge AJ, Downie RC, Benbow HR, Barker GL, Wilkinson PA, Coghill J, Waterfall C, Davassi A *et al.* 2017. Characterization of a Wheat Breeders' Array suitable for high-throughput SNP genotyping of global accessions of hexaploid bread wheat (*Triticum aestivum*). *Plant Biotechnology Journal* **15**: 390–401.

Armstrong SJ, Caryl AP, Jones GH, Franklin FC. 2002. Asy1, a protein required for meiotic chromosome synapsis, localizes to axis-associated chromatin in Arabidopsis and Brassica. *Journal of Cell Science* **115**: 3645–3655.

Arrieta M, Macaulay M, Colas I, Schreiber M, Shaw PD, Waugh R, Ramsay L. 2021. An induced mutation in HvRECQL4 increases the overall recombination and restores fertility in a barley HvMLH3 mutant background. *Frontiers in Plant Science* **12**: 706560.

Berchowitz LE, Francis KE, Bey AL, Copenhaver GP. 2007. The role of AtMUS81 in interference-insensitive crossovers in *A. thaliana*. *PLoS Genetics* **3**: e132.

Blary A, Jenczewski E. 2019. Manipulation of crossover frequency and distribution for plant breeding. *Theoretical and Applied Genetics* **132**: 575–592.

Börner GV, Kleckner N, Hunter N. 2004. Crossover/noncrossover differentiation, synaptonemal complex formation, and regulatory surveillance at the leptotene/zygotene transition of meiosis. *Cell* **117**: 29–45.

Capilla-Pérez L, Durand S, Hurel A, Lian Q, Chambon A, Taochy C, Solier V, Grelon M, Mercier R. 2021. The synaptonemal complex imposes crossover interference and heterochiasmy in Arabidopsis. *Proceedings of the National Academy of Sciences, USA* **118**: e2023613118.

Chelysheva L, Gendrot G, Vezon D, Doutriaux M-P, Mercier R, Grelon M. 2007. Zip4/Spo22 is required for class I CO formation but not for synapsis completion in *Arabidopsis thaliana*. *PLoS Genetics* **3**: e83.

Chelysheva L, Vezon D, Chambon A, Gendrot G, Pereira L, Lemhemdi A, Vrielynck N, Le Guin S, Novatchkova M, Grelon M. 2012. The Arabidopsis HEI10 is a new ZMM protein related to Zip3. *PLoS Genetics* **8**: e1002799.

Choulet F, Alberti A, Theil S, Glover N, Barbe V, Daron J, Pingault L, Sourdille P, Couloux A, Paux E *et al.* 2014. Structural and functional partitioning of bread wheat chromosome 3B. *Science* **345**: 1249721.

Crismani W, Girard C, Froger N, Pradillo M, Santos JL, Chelysheva L, Copenhaver GP, Horlow C, Mercier R. 2012. FANCM limits meiotic crossovers. *Science* **336**: 1588–1590.

Desjardins SD, Ogle DE, Ayoub MA, Heckmann S, Henderson IR, Edwards KJ, Higgins JD. 2020. MutS homologue 4 and MutS homologue 5 maintain the obligate crossover in wheat despite stepwise gene loss following polyploidization. *Plant Physiology* **183**: 1545–1558.

Desjardins SD, Simmonds J, Guterman I, Kanyuka K, Burridge AJ, Tock AJ, Sanchez-Moran E, Franklin FCH, Henderson IR, Edwards KJ *et al.* 2022. FANCM promotes class I interfering crossovers and suppresses class II non-interfering crossovers in wheat meiosis. *Nature Communications* **13**: 3644.

Durand S, Lian Q, Jing J, Ernst M, Grelon M, Zwicker D, Mercier R. 2022. Joint control of meiotic crossover patterning by the synaptonemal complex and HEI10 dosage. *Nature Communications* **13**: 5999.

Fernandes JB, Duhamel M, Seguéla-Arnaud M, Froger N, Girard C, Choinard S, Solier V, De Winne N, De Jaeger G, Gevaert K *et al.* 2018a. FIGL1 and its novel partner FLIP form a conserved complex that regulates homologous recombination. *PLoS Genetics* **14**: e1007317.

Fernandes JB, Séguéla-Arnaud M, Larchevêque C, Lloyd AH, Mercier R. 2018b. Unleashing meiotic crossovers in hybrid plants. *Proceedings of the National Academy of Sciences, USA* **115**: 2431–2436.

France MG, Enderle J, Röhrig S, Puchta H, Franklin FCH, Higgins JD. 2021. ZYP1 is required for obligate cross-over formation and cross-over interference in Arabidopsis. *Proceedings of the National Academy of Sciences, USA* **118**: e2021671118.

Gardiner LJ, Wingen LU, Bailey P, Joynson R, Brabbs T, Wright J, Higgins JD, Hall N, Griffiths S, Clavijo BJ *et al.* 2019. Analysis of the recombination landscape of hexaploid bread wheat reveals genes controlling recombination and gene conversion frequency. *Genome Biology* **20**: 69.

Girard C, Chelysheva L, Choinard S, Froger N, Macaisne N, Lemhemdi A, Mazel J, Crismani W, Mercier R. 2015. AAA-ATPase FIDGETIN-LIKE 1 and helicase FANCM antagonize meiotic crossovers by distinct mechanisms. *PLoS Genetics* **11**: e1005369.

Haering CH, Jessberger R. 2012. Cohesin in determining chromosome architecture. *Experimental Cell Research* **318**: 1386–1393.

Hesse S, Zelkowski M, Mikhailova EI, Keijzer CJ, Houben A, Schubert V. 2019. Ultrastructure and dynamics of synaptonemal complex components during meiotic pairing and synapsis of standard (A) and accessory (B) rye chromosomes. *Frontiers in Plant Science* **10**: 773.

Higgins JD, Armstrong SJ, Franklin FC, Jones GH. 2004. The Arabidopsis MutS homolog AtMSH4 functions at an early step in recombination: evidence for two classes of recombination in Arabidopsis. *Genes & Development* **18**: 2557–2570.

Higgins JD, Buckling EF, Franklin FC, Jones GH. 2008a. Expression and functional analysis of AtMUS81 in Arabidopsis meiosis reveals a role in the second pathway of crossing-over. *The Plant Journal* **54**: 152–162.

Higgins JD, Osman K, Desjardins SD, Henderson IR, Edwards KJ, Franklin FCH. 2022. Unravelling mechanisms that govern meiotic crossover formation in wheat. *Biochemical Society Transactions* **50**: 1179–1186.

Higgins JD, Perry RM, Barakate A, Ramsay L, Waugh R, Halpin C, Armstrong SJ, Franklin FC. 2012. Spatiotemporal asymmetry of the meiotic program underlies the predominantly distal distribution of meiotic crossovers in barley. *Plant Cell* **24**: 4096–4109.

Higgins JD, Sanchez-Moran E, Armstrong SJ, Jones GH, Franklin FC. 2005. The Arabidopsis synaptonemal complex protein ZYP1 is required for chromosome synapsis and normal fidelity of crossing over. *Genes & Development* **19**: 2488–2500.

Higgins JD, Vignard J, Mercier R, Pugh AG, Franklin FC, Jones GH. 2008b. AtMSH5 partners AtMSH4 in the class I meiotic crossover pathway in *Arabidopsis thaliana*, but is not required for synapsis. *The Plant Journal* **55**: 28–39.

Hu Q, Li Y, Wang H, Shen Y, Zhang C, Du G, Tang D, Cheng Z. 2017. Meiotic chromosome association 1 interacts with TOP3α and regulates meiotic recombination in rice. *Plant Cell* **29**: 1697–1708.

International Wheat Genome Sequencing CI. 2018. Shifting the limits in wheat research and breeding using a fully annotated reference genome. *Science* **361**: eaar7191.

International Wheat Genome Sequencing Consortium (IWGSC), Mayer KFX, Rogers J, Doležel J, Pozniak C, Eversole K, Feuillet C, Gill B, Friebe B, Lukaszewski AJ *et al.* 2014. A chromosome-based draft sequence of the hexaploid bread wheat (*Triticum aestivum*) genome. *Science* **345**: 1251788.

Ito M, Furukohri A, Matsuzaki K, Fujita Y, Toyoda A, Shinohara A. 2023. FIGNL1 AAA+ ATPase remodels RAD51 and DMC1 filaments in pre-meiotic DNA replication and meiotic recombination. *Nature Communications* **14**: 6857.

Ji J, Tang D, Shen Y, Xue Z, Wang H, Shi W, Zhang C, Du G, Li Y, Cheng Z. 2016. P31comet, a member of the synaptonemal complex, participates in meiotic DSB formation in rice. *Proceedings of the National Academy of Sciences, USA* **113**: 10577–10582.

Jones GH, Franklin FC. 2006. Meiotic crossing-over: obligation and interference. *Cell* **126**: 246–248.

Keeney S, Giroux CN, Kleckner N. 1997. Meiosis-specific DNA double-strand breaks are catalyzed by Spo11, a member of a widely conserved protein family. *Cell* **88**: 375–384.

Knoll A, Higgins JD, Seeliger K, Reha SJ, Dangel NJ, Bauknecht M, Schröpfer S, Franklin FC, Puchta H. 2012. The Fanconi anemia ortholog FANCM ensures ordered homologous recombination in both somatic and meiotic cells in Arabidopsis. *Plant Cell* **24**: 1448–1464.

Krasileva KV, Vasquez-Gross HA, Howell T, Bailey P, Paraiso F, Clissold L, Simmonds J, Ramirez-Gonzalez RH, Wang X, Borrill P *et al.* 2017. Uncovering hidden variation in polyploid wheat. *Proceedings of the National Academy of Sciences, USA* **114**: E913–E921.

Kumar R, Duhamel M, Coutant E, Ben-Nahia E, Mercier R. 2019. Antagonism between BRCA2 and FIGL1 regulates homologous recombination. *Nucleic Acids Research* **47**: 5170–5180.

Lück S, Kreszies T, Strickert M, Schweizer P, Kuhlmann M, Douchkov D. 2019. siRNA-Finder (si-Fi) Software for RNAi-target design and off-target prediction. *Frontiers in Plant Science* **10**: 1023.

Macaisne N, Novatchkova M, Peirera L, Vezon D, Jolivet S, Froger N, Chelysheva L, Grelon M, Mercier R. 2008. SHOC1, an XPF endonuclease-related protein, is essential for the formation of class I meiotic crossovers. *Current Biology* **18**: 1432–1437.

Macaisne N, Vignard J, Mercier R. 2011. SHOC1 and PTD form an XPF-ERCC1-like complex that is required for formation of class I crossovers. *Journal of Cell Science* **124**: 2687–2691.

Maccaferri M, Harris NS, Twardziok SO, Pasam RK, Gundlach H, Spannagl M, Ormanbekova D, Lux T, Prade VM, Milner SG *et al.* 2019. Durum wheat genome highlights past domestication signatures and future improvement targets. *Nature Genetics* **51**: 885–895.

Martini E, Diaz RL, Hunter N, Keeney S. 2006. Crossover homeostasis in yeast meiosis. *Cell* **126**: 285–295.

Mercier R, Jolivet S, Vezon D, Huppe E, Chelysheva L, Giovanni M, Nogué F, Doutriaux MP, Horlow C, Grelon M *et al.* 2005. Two meiotic crossover classes cohabit in Arabidopsis: one is dependent on MER3, whereas the other one is not. *Current Biology* **15**: 692–701.

Mercier R, Mézard C, Jenczewski E, Macaisne N, Grelon M. 2015. The molecular biology of meiosis in plants. *Annual Review of Plant Biology* **66**: 297–327.

Mieulet D, Aubert G, Bres C, Klein A, Droc G, Vieille E, Rond-Coissieux C, Sanchez M, Dalmais M, Mauxion JP *et al.* 2018. Unleashing meiotic crossovers in crops. *Nature Plants* **4**: 1010–1016.

Nageswaran DC, Kim J, Lambing C, Kim J, Park J, Kim EJ, Cho HS, Kim H, Byun D, Park YM *et al.* 2021. HIGH CROSSOVER RATE1 encodes PROTEIN PHOSPHATASE X1 and restricts meiotic crossovers in Arabidopsis. *Nature Plants* **7**: 452–467.

Osman K, Algopishi U, Higgins JD, Henderson IR, Edwards KJ, Franklin FCH, Sanchez-Moran E. 2021. Distal bias of meiotic crossovers in hexaploid bread wheat reflects spatio-temporal asymmetry of the meiotic program. *Frontiers in Plant Science* **12**: 631323.

Osman K, Higgins JD, Sanchez-Moran E, Armstrong SJ, Franklin FCH. 2011. Pathways to meiotic recombination in *Arabidopsis thaliana*. *New Phytologist* **190**: 523–544.

Osman K, Yang J, Roitinger E, Lambing C, Heckmann S, Howell E, Cuacos M, Imre R, Dürnberger G, Mechtler K *et al.* 2018. Affinity proteomics reveals extensive phosphorylation of the *Brassica* chromosome axis protein ASY1 and a network of associated proteins at prophase I of meiosis. *The Plant Journal* **93**: 17–33.

Page SL, Hawley RS. 2004. The genetics and molecular biology of the synaptonemal complex. *Annual Review of Cell and Developmental Biology* **20**: 525–558.

Saintenac C, Falque M, Martin OC, Paux E, Feuillet C, Sourdille P. 2009. Detailed recombination studies along chromosome 3B provide new insights on crossover distribution in wheat (*Triticum aestivum* L.). *Genetics* **181**: 393–403.

Séguéla-Arnaud M, Crismani W, Larchevêque C, Mazel J, Froger N, Choinard S, Lemhemdi A, Macaisne N, Van Leene J, Gevaert K *et al.* 2015. Multiple mechanisms limit meiotic crossovers: TOP3α and two BLM homologs antagonize crossovers in parallel to FANCM. *Proceedings of the National Academy of Sciences, USA* **112**: 4713–4718.

Serra H, Lambing C, Griffin CH, Topp SD, Nageswaran DC, Underwood CJ, Ziolkowski PA, Séguéla-Arnaud M, Fernandes JB, Mercier R *et al.* 2018. Massive crossover elevation via combination of HEI10 and recq4a recq4b during Arabidopsis meiosis. *Proceedings of the National Academy of Sciences, USA* **115**: 2437–2442.

Shorinola O, Simmonds J, Wingen LU, Uauy C. 2022. Trend, population structure, and trait mapping from 15 years of national varietal trials of UK winter wheat. *G3: Genes, Genomes, Genetics* **12**: jkab415.

Uauy C, Wulff BBH, Dubcovsky J. 2017. Combining traditional mutagenesis with new high-throughput sequencing and genome editing to reveal hidden variation in polyploid wheat. *Annual Review of Genetics* **51**: 435–454.

Vrielynck N, Chambon A, Vezon D, Pereira L, Chelysheva L, De Muyt A, Mézard C, Mayer C, Grelon M. 2016. A DNA topoisomerase VI-like complex initiates meiotic recombination. *Science* **351**: 939–943.

Wang K, Wang M, Tang D, Shen Y, Miao C, Hu Q, Lu T, Cheng Z. 2012. The role of rice HEI10 in the formation of meiotic crossovers. *PLoS Genetics* **8**: e1002809.

Wang Y, Copenhaver GP. 2018. Meiotic recombination: mixing it up in plants. *Annual Review of Plant Biology* **69**: 577–609.

Wijeratne AJ, Chen C, Zhang W, Timofejeva L, Ma H. 2006. The *Arabidopsis thaliana* PARTING DANCERS gene encoding a novel protein is required for normal meiotic homologous recombination. *Molecular Biology of the Cell* **17**: 1331–1343.

Yang S, Zhang C, Cao Y, Du G, Tang D, Li Y, Shen Y, Yu H, Cheng Z. 2022. FIGNL1 inhibits non-homologous chromosome association and crossover formation. *Frontiers in Plant Science* **13**: 945893.

Yuan C, Li C, Yan L, Jackson AO, Liu Z, Han C, Yu J, Li D. 2011. A high throughput barley stripe mosaic virus vector for virus induced gene silencing in monocots and dicots. *PLoS ONE* **6**: e26468.

Yuan J, Chen J. 2013. FIGNL1-containing protein complex is required for efficient homologous recombination repair. *Proceedings of the National Academy of Sciences, USA* **110**: 10640–10645.

Zhang P, Zhang Y, Sun L, Sinumporn S, Yang Z, Sun B, Xuan D, Li Z, Yu P, Wu W *et al.* 2017. The rice AAA-ATPase OsFIGNL1 is essential for male meiosis. *Frontiers in Plant Science* **8**: 1639.

Zhang Q, Fan J, Xu W, Cao H, Qiu C, Xiong Y, Zhao H, Wang Y, Huang J, Yu C. 2023. The FLIP-FIGNL1 complex regulates the dissociation of RAD51/DMC1 in homologous recombination and replication fork restart. *Nucleic Acids Research* **51**: 8606–8622.

Zhang T, Zhao SH, Wang Y, He Y. 2023. FIGL1 coordinates with dosage-sensitive BRCA2 in modulating meiotic recombination in maize. *Journal of Integrative Plant Biology* **65**: 2107–2121.

Zickler D, Kleckner N. 2023. Meiosis: dances between homologs. *Annual Review of Genetics* **57**: 1–63.

Ziolkowski PA, Underwood CJ, Lambing C, Martinez-Garcia M, Lawrence EJ, Ziolkowska L, Griffin C, Choi K, Franklin FC, Martienssen RA *et al.* 2017. Natural variation and dosage of the HEI10 meiotic E3 ligase control Arabidopsis crossover recombination. *Genes & Development* **31**: 306–317.

Supporting Information

Additional Supporting Information may be found online in the Supporting Information section at the end of the article.

Fig. S1 Clustal Omega Multiple Sequence Alignment of wheat FIGL1 predicted proteins.

Fig. S2 EMBOSS Needle pairwise alignments of TaFIGL1 protein consensus sequence with rice and Arabidopsis orthologues.

Fig. S3 Abnormal tetrads from *Tafigl1* with unbalanced, micro- and poly-nuclei.

Fig. S4 Cytological analysis of progeny from *Tafigl1* selfing.

Table S1 B genome FIGL1 region scaffold original output.

Table S2 Summary of selected *figl1* mutants.

Table S3 Skyfall × Cadenza recombination analysis data.

Please note: Wiley is not responsible for the content or functionality of any Supporting Information supplied by the authors. Any queries (other than missing material) should be directed to the *New Phytologist* Central Office.